Interactions of Semiflexible Filaments and Molecular Motors

Dmitry Karpeev,[1] Igor S. Aranson,[2] Lev S. Tsimring,[3] and Hans G. Kaper[4]

[1]*Mathematics and Computer Science Division, Argonne National Laboratory, 9700 South Cass Avenue, Argonne, IL 60439*
[2]*Materials Science Division, Argonne National Laboratory, 9700 South Cass Avenue, Argonne, IL 60439*
[3]*Institute for Nonlinear Science, University of California at San Diego, 9500 Gilman Drive, La Jolla, CA 92093*
[4]*Mathematics and Computer Science Division, Argonne National Laboratory, 9700 South Cass Avenue, Argonne, IL 60439; current address: Division of Mathematical Sciences, National Science Foundation, 4201 Wilson Blvd., Arlington, VA 22230*

(Dated: December 13, 2006)

This paper summarizes the results of numerical simulations of the interaction of a pair of biofilaments mediated by a molecular motor. The filaments are modeled as flexible rods, and the results are applicable to microtubules, which are relatively stiff, as well as to much softer filaments, such as actin. The results provide insight into the effects of flexibility on cytoskeleton formation and the rheology of semiflexible filament networks. The simulations are based on a nonlinear elasticity equation. The results show that flexibility enhances the tendency of the filaments to align. The enhancement in turn favors the formation of large-scale structures in multifilament systems. Simulations for soft filaments show that the action of the motor can result in the formation of multiple loops of the filaments as a result of buckling.

PACS numbers: 87.16.-b, 05.65.+b,47.55.+r

I. INTRODUCTION

One of the primary functions of molecular motors is to form complex networks of long biofilaments (microtubules, actin, and others) and organize the cytoskeleton of daughter cells during cell division [1]. *In vitro* experiments of the interaction of molecular motors and microtubules [2–7] performed in isolation from other biophysical processes that normally occur simultaneously *in vivo* have shown that, at sufficiently large concentrations of the molecular motors and microtubules, the latter self-organize in starlike *asters* and rotating *vortices*, depending on the type and concentration of the molecular motors.

This phenomenon of pattern formation in mixtures of microtubules and molecular motors can be studied in a multiscale framework. In [8, 9] we developed a mesoscopic theory to explain the alignment of the microtubules (see also Ref. [10]). The theory is based on a stochastic master equation that governs the evolution of the probability density of microtubules with a given orientation at a given location. Binary interactions of microtubules are considered as instantaneous *collisions* that are mediated by uniformly distributed motors. In this mesoscopic theory, the details of the interaction kernel are assumed to be known and derived from a microscopic theory. In the present paper we consider such a microscopic theory. In particular, we are interested in quantifying the effects of flexibility of the filaments on the interaction kernel.

Experiments [4–7] suggest the following qualitative picture of motor–filament interactions. If a free molecular motor binds to a microtubule at a random position, it marches along the filament in a fixed direction until it unbinds, perhaps after a period of *dwelling* at the end of the filament, as for ncd-type motors. The position and orientation of the filament are essentially unchanged by the process, since the mass of the molecular motor is small in comparison with that of the microtubule. However, if a molecular motor binds to two microtubules (most molecular motors have at least two binding sites), it can change the relative position and orientation of the filaments significantly. The two-dimensional case is illustrated in Fig. 1a. Before the interaction, the microtubules are oriented at angles $\varphi_{1,b}$ and $\varphi_{2,b}$. The simultaneous binding of the molecular motor to the two microtubules results in a complete alignment of the latter; after the interaction the microtubules are oriented at angles $\varphi_{1,a}$ and $\varphi_{2,a}$, where $\varphi_{1,a} = \varphi_{2,a} = \frac{1}{2}(\varphi_{1,b} + \varphi_{2,b})$. We refer to this type of interaction as a *fully inelastic collision*, by analogy with the physics of inelastically colliding grains; see, for example, Ref. [11].. In [8, 9] we showed that these inelastic collisions can lead to an orientational instability and a subsequent local ordering of filaments. The orientational instability can be compared to the clustering instability in dissipative granular gases [12].

While a fully inelastic collision appears to be a simple and useful approximation, the details of the interaction of two microtubules mediated by a molecular motor are more complicated. A useful parameter to characterize the inelasticity of the collision is the *inelasticity factor* ϵ,

$$\epsilon = \varphi_f/\varphi_0, \tag{1}$$

where φ_f is the angle between the filaments after the interaction, $\varphi_f = |\varphi_{1,a} - \varphi_{2,a}|$, and φ_0 the angle before the interaction, $\varphi_0 = |\varphi_{1,b} - \varphi_{2,b}|$. Thus, $\epsilon = 0$ for a fully inelastic collision ($\varphi_{1,a} = \varphi_{2,a}$) and $\epsilon = 1$ for an elastic collision ($\varphi_f = \varphi_0$).

A micromechanical calculation [9] shows that for pairs of *rigid* filaments the interaction mediated by a molecular motor is only partially inelastic and, in fact, depends

on the position of the initial attachment point on the tubule. A more meaningful concept is therefore the *mean inelasticity factor* $\bar{\epsilon}$,

$$\bar{\epsilon} = \frac{\langle \varphi_f \rangle}{\varphi_0}. \tag{2}$$

Here the average is taken over all possible initial attachment positions; for filaments of length L,

$$\langle \varphi_f \rangle = L^{-1} \int_{-L/2}^{L/2} \varphi_f(s) ds. \tag{3}$$

Thus, $\bar{\epsilon} = 0$ for fully inelastic interactions, $\bar{\epsilon} = 1$ for fully elastic interactions.

The mean inelasticity factor $\bar{\epsilon}$ is a complicated nonlinear function of φ_0, but a good approximation for rigid filaments and small φ_0 is

$$\bar{\epsilon} \approx \frac{1}{2} + \frac{\operatorname{arcsinh}(\sqrt{\kappa}/2)}{\sqrt{\kappa(1+\kappa/4)}}. \tag{4}$$

Here κ measures the ratio of the translational and rotational viscous drag coefficients, $\kappa = (\xi_\parallel/\xi_r)L^2$ for tubules of length L. Numerically, κ is in the range of 12 to 15, so $\bar{\epsilon} \approx 0.63$ for rigid rods at small angles [9].

The sensitivity of the inelasticity to the initial attachment point is measured by the *asymmetry coefficient* $\bar{\alpha}$,

$$\bar{\alpha} = \frac{\langle s\varphi_f \rangle}{L\langle \varphi_f \rangle}. \tag{5}$$

For rigid rods, $\varphi_f(s) = \varphi_f(-s)$, so $\bar{\alpha} = 0$. Note that the asymmetry coefficient differs from the collision kernel anisotropy introduced in Ref. [9]. The latter is related to the motor dwelling time at the end of microtubules; however, we anticipate that a strong asymmetry $\bar{\alpha}$ has a similar effect on pattern formation as does the kernel anisotropy and, for example, favors the formation of asters over vortices. Together, the two parameters $\bar{\epsilon}$ and $\bar{\alpha}$ determine the collision kernel in the mesoscopic theory [9].

The purpose of this investigation is to study the mean inelasticity factor and asymmetry coefficients of interacting filaments with various degrees of *flexibility*. Using the continuum nonlinear elasticity equations, we show through numerical simulations that a finite bending flexibility amplifies the inelasticity of the collisions. While microtubules are practically unbendable by thermal fluctuations, molecular motors can bend them easily. Bending also increases the probability that two motors attach themselves simultaneously to two microtubules at different positions. When this situation happens, the motors cross-link the microtubules, making them exactly parallel and thus realizing a fully inelastic collision, $\bar{\epsilon} = 0$. Further simulations for more flexible biofilaments, such as actin, reveal an unexpected buckling instability and the formation of multiple loops. These results provide insight into the effects of flexibility on cytoskeleton formation and the rheology of semiflexible filament networks.

Section II describes details of the mathematical model underlying the numerical simulations. Section III summarizes the results of the numerical simulations for both microtubules and soft filaments. Section IV describes our conclusions. Two appendices contain technical details about the kinematics of filament interactions mediated by molecular motors (Appendix A) and the discretization of the mathematical model (Appendix B).

II. MODEL

Consider the interaction of two semiflexible rods (microtubules or, more generally, biofilaments) mediated by a molecular motor. We assume that the microtubules are of equal length L, where L is constant in time. (That is, we focus on the case where the endpoints of the microtubules are stabilized, for example with taxol, so that polymerization and depolymerization processes, which may affect the lengths of the microtubules, are insignificant.) We assume furthermore for simplicity that the molecular motor attaches *symmetrically* to the microtubules. Thus, the two attachment points are at the same position on each rod with respect to their respective midpoints, and the force exerted by the motor is perpendicular to the bisector of the microtubule pair; see Fig. 1b. The last conclusion follows from the assumption that the motor, while moving along the filaments with a constant speed, acts as a strong spring bringing the two ends together. In Appendix A we show that the motor has a tendency to orient perpendicular to the bisector of the microtubule pair even if the motor has a nonzero length. Since the initial attachment may occur at a random position on the tubule, we are interested in the properties of the interaction (in particular, the inelasticity coefficient) *averaged* with respect to the initial attachment position. We make the natural assumption that the probability of attachment is distributed uniformly along a microtubule. We neglect the effects of thermal fluctuations on the microtubule shape, since the thermal persistence length of the microtubules is very large (several millimeters). However, thermal fluctuations may have some effect on the shape of much softer biofilaments such as actin, whose thermal persistence length is of the order of a few microns.

A. Kinematics

To describe the motion of interlinked microtubules, we combine the theory of Refs. [13, 14] for a semiflexible polymer with the analysis of the rigid case in Ref. [9]. We adopt a two-dimensional setting and model a microtubule

as a semiflexible homogeneous inextensible elastic rod of length L and bending stiffness β. We measure locations along the rod relative to the rod's midpoint, using the arclength s as the natural parameter, so $-\frac{1}{2}L \leq s \leq \frac{1}{2}L$; see Fig. 1b. The inextensibility of the rod implies that the embedding preserves arclength elements. Thus, if $\mathbf{r}(s)$ is the position vector at the point s on the tubule and $\mathbf{r}_s$ denotes its derivative with respect to s, then we have the local constraint $\mathbf{r}_s \cdot \mathbf{r}_s = 1$.

A molecular motor attaches initially to the tubule at the point s_i and moves along the tubule with the constant velocity v, exerting a force $\mathbf{f}$ on the tubule. As long as the force does not exceed a critical value, we may assume that the velocity of the motor does not depend on the force $\mathbf{f}$. However, we emphasize that this assumption is not essential; similar calculations can be carried out if the motor velocity depends on the force. Since the velocity is fixed, the movement of the attachment point s_a is subject to the kinematic constraint

$$s_a(t) = s_i + vt. \tag{6}$$

In a binary collision, the molecular motor attaches to and moves along two microtubules simultaneously, and the relative configuration of the tubules changes due to the motor force acting on both tubules. As explained above, we consider only symmetric interactions, where the force is normal to the bisector. Then we can select a Cartesian coordinate system where the y-axis is directed along the bisector (see Fig. 1b), so $\mathbf{f} = (\pm f, 0)$, where the magnitude f of $\mathbf{f}$ has to be deduced from the kinematic constraint.

B. Governing Equations

The equations governing the motion of the microtubules are derived from the balance of forces. If the viscosity of the medium containing the mixture is large (Stokes limit), then the viscous drag force is balanced by the force acting on the tubules. The latter is the variational derivative of the energy functional E measuring the bending energy of the tubule, together with the inextensibility and the motor attachment constraints,

$$E = \int_{-L/2}^{L/2} \Big(g(\mathbf{r}_s \cdot \mathbf{r}_s - 1) + \beta \mathbf{r}_{ss} \cdot \mathbf{r}_{ss} + \mathbf{f} \cdot \mathbf{r}\, \delta(s - s_a) \Big) ds. \tag{7}$$

Here, g is the line tension, which is determined implicitly from the length conservation constraint $|\mathbf{r}_s|^2 = 1$. The singular component of the energy is due to the kinematic constraint, Eq. (6), and the choice of a moving coordinate system that places the origin at the motor attachment point $\mathbf{r}(s_a)$. The equations of motion are found by taking variations,

$$\eta \dot{\mathbf{r}} = -\frac{\delta E}{\delta \mathbf{r}}, \quad 0 = -\frac{\delta E}{\delta g}, \quad 0 = -\frac{\delta E}{\delta f}. \tag{8}$$

Here, η is the viscous drag coefficient (per unit length). These equations can be interpreted as defining a gradient flow with respect to the variables $\mathbf{r}$, g, and $\mathbf{f}$, where the constraints are established instantaneously on the time scale of the viscous force.

The solution of Eqs. (8) must satisfy the integral relation

$$\int_{-L/2}^{L/2} \Big(\eta \dot{\mathbf{r}} \cdot \delta \mathbf{r} + \delta E \Big) ds = 0,$$

for all admissible variations $\delta \mathbf{r}$, δg and δf. The energy variation is

$$\delta E = \int_{-L/2}^{L/2} \Big(g \mathbf{r}_s \cdot \delta \mathbf{r}_s + \beta \mathbf{r}_{ss} \cdot \delta \mathbf{r}_{ss} + \frac{1}{2} \delta(s - s_a) \mathbf{f} \cdot \delta \mathbf{r} \Big) ds + \int_{-L/2}^{L/2} \Big(\mathbf{r}_s \cdot \mathbf{r}_s - 1 \Big) \delta g \, ds + \int_{-L/2}^{L/2} \mathbf{r} \delta(s - s_a) \cdot \delta \mathbf{f} ds.$$

We obtain the *weak form* of the governing equations by assuming that the variations are independent,

$$\int_{-L/2}^{L/2} \Big[\eta \dot{\mathbf{r}} \cdot \delta \mathbf{r} + g \mathbf{r}_s \cdot \delta \mathbf{r}_s + \beta \mathbf{r}_{ss} \cdot \delta \mathbf{r}_{ss} + \frac{1}{2} \delta(s - s_a) \mathbf{f} \cdot \delta \mathbf{r} \Big] ds = 0, \tag{9}$$

$$\int_{-L/2}^{L/2} (\mathbf{r}_s \cdot \mathbf{r}_s - 1) \, \delta g \, ds = 0, \quad \int_{-L/2}^{L/2} \delta(s - s_a) \mathbf{r} \cdot \delta \mathbf{f} ds = 0. \tag{10}$$

In this weak formulation there is no need for a priori assumptions on the smoothness of the solutions and their boundary conditions. However, if the solution is sufficiently smooth, we can integrate by parts and obtain the *strong form* of the governing equations,

$$\int_{-L/2}^{L/2} \Big[\eta \dot{\mathbf{r}} - \partial_s (g \mathbf{r}_s) + \beta \partial_s^4 \mathbf{r} + \frac{1}{2} \delta(s - s_a) \mathbf{f} \Big] \cdot \delta \mathbf{r} ds + \Big[g \mathbf{r}_s \cdot \delta \mathbf{r} + \beta \mathbf{r}_{ss} \cdot \delta \mathbf{r}_s - \beta \mathbf{r}_{sss} \cdot \delta \mathbf{r} \Big]_{-L/2}^{L/2} = 0.$$

The vanishing of the integral is equivalent to the equations of motion in the usual differential form (8), while the vanishing of the boundary term determines the natural boundary conditions,

$$g \mathbf{r}_s \cdot \delta \mathbf{r} + \beta \mathbf{r}_{ss} \cdot \delta \mathbf{r}_s - \beta \mathbf{r}_{sss} \cdot \delta \mathbf{r} + \frac{1}{2} \delta_{s_a, s_b} \mathbf{f} \cdot \delta \mathbf{r} = 0 \tag{11}$$

at each boundary point $s_b = \pm L/2$. The Kronecker delta symbol δ_{s_a, s_b} ensures the inclusion of the force in the boundary condition when the motor is attached at the boundary.

In the absence of smoothness assumptions, Eqs. (9)–(10) implicitly contain the suitable weak version of the boundary conditions. In particular, the formulation (9)–(10) does not change when $s_a = \pm L/2$, while for the equation above the term $\mathbf{f}$ becomes part of the boundary conditions.

The weak formulation is amenable to discretization in the presence of singular terms. One such term appears in the equation of motion for $\mathbf{r}$ as a result of the movable point force exerted by the motor. If an explicit equation of motion for the tension g is derived from the inextensibility constraint and the equations of motion for $\mathbf{r}$, an even more cumbersome singular term appears:

$$g_{ss} - \mathbf{r}_{ss}\cdot\mathbf{r}_{ss}g - \beta\mathbf{r}_s\partial_s^5\mathbf{r} + \frac{1}{2}\mathbf{r}_s\mathbf{f}\delta'(s-s_a) = 0. \qquad (12)$$

This equation demands even higher regularity of $\mathbf{r}$ than the equation for $\mathbf{r}$ itself. We circumvent both problems by solving the constraints rather than deriving explicit equations for the forces of constraints. The result is a well-posed discrete problem that, however, requires an implicit time discretization; see Appendix B for details.

III. NUMERICAL EXPERIMENTS

Symmetric interactions of pairs of microtubules are simulated numerically by integrating the equations of motion (9)–(10). In this section we present the results of two types of such simulations, first for (relatively stiff) microtubules and then for (fairly soft) actin filaments.

Physical parameters. The viscous drag coefficient per unit length, η, is related to the effective dynamic viscosity of the solvent, μ; in a thin layer of solvent the approximate relation is $\eta \approx 2\pi\mu/\ln(\tilde{L}/d)$, where $\tilde{L}$ is a characteristic cut-off size of the problem (for example, the average filament length or the depth of the container), typically of the order 5 microns. This models the proximity of the container walls above and below the tubules (see also Refs. [5, 15, 16]). The bulk dynamic viscosity coefficient for water, the assumed solvent, is $\mu = 10^{-3}$ pN s μm^{-2}. Moreover, viscosity can increase significantly as a result of the presence of various organic additives, such as motors and adenosine triphosphate. To account for these effects, we use the effective drag coefficient $\eta = 3\mu = 3\times10^{-3}$pN s μm^2.

We use a microtubule bending stiffness strength $\beta = 2.0\times10^{-23}Nm^2 = 20$ pN μm^2, as calculated in [15]. The motor velocity is set to $v = 1\,\mu$m/s [5]. Note that by scaling space (hence the microtubule length) by λ, the effective bending stiffness is scaled by λ^{-4}, while the tension g and the force $\mathbf{f}$ (Lagrange multipliers) remain unchanged. Thus, we normalize space so that each tubule is of unit length. Time is normalized by using T, the length of time needed for the motor to traverse 1 μm ($T = 1$ s in our case), resulting in a nondimensional motor velocity $\hat{v} = vT/L$.

Effective bending stiffness. The introduction of an effective bending stiffness, $\hat{\beta} = \beta L^{-4}\eta^{-1}T$, enables us to study the interactions of a range of tubules of different lengths by means of a single tubule of unit length but with different values for the effective bending stiffness and motor velocity. Thus there is no need to change the spatial discretization of the microtubule to maintain accuracy.

Discretization parameters. In all simulations, we discretized the normalized tubule of length 1 with $\Delta s = 0.03125$ or smaller and time with $\Delta t = 0.01$. Simulations of tubules of different lengths ($L = 15, 30, 45, 60$ μm) were accomplished by adjusting the effective bending stiffness (as explained in the previous paragraph), $\hat{\beta} = 1.32\times10^{-1}, 8.23\times10^{-3}, 1.63\times10^{-3}, 5.14\times10^{-4}$; the effective drag coefficient, $\hat{\eta} = 1.0$; and the effective motor velocity, $\hat{v} = 0.067, 0.033, 0.022, 0.017$.

After the interaction, the tubule is allowed to relax until the mean relative deviation of the tangent from the mean is less than 10^{-2}. This process was done in two different ways, with the motor sliding off the tubule and with the motor dwelling at the end of the tubule, until the relaxation is complete. The dwelling was introduced to model different types of motors. It is known that some motors, such as kinesin, have almost zero dwelling time, whereas the NCD-type motor complexes used in experimental works (see Refs. [4, 5]) appear to have a very large dwelling time at the microtubule ends.

A. Bending of Microtubules

Figure 2 shows two typical examples of the time evolution of the interaction of a pair of relatively stiff microtubules mediated by a molecular motor. In both cases, the motor induces significant deformation of the filament shape. The tubules curve in such a way that the segments of microtubules behind the moving motor become more aligned than if the tubules were straight. This curvature increases the probability of attachment of additional motors and, therefore, the probability of cross-linking of the tubules in several places. Multiple cross-linking is expected to quickly align the two tubules; however, a consideration of the action of multiple motors is well beyond the scope of the present work.

Figure 3 shows the evolution of the filament tension $g(s)$ in the course of the interaction. The filaments become stretched ($g > 0$) ahead of the motor attachment point ($s > s_a$) and slightly compressed ($g < 0$) behind the attachment point ($s < s_a$). In the limit of zero motor size, the tension exhibits a discontinuity at the attachment point ($s = s_a$) because of the δ-function character of the motor force $\mathbf{f}$. In our numerical procedure this discontinuity is regularized as a result of the finite discretization mesh (equivalently, the finite size of the motor). The negative tension g is a precursor of the Euler buckling instability for elastic rods [17]. However, the buckling of microtubules does not occur because of the very large value of the stiffness coefficient β.

Figures 4–7 show the results for the inelasticity factor $\bar{\epsilon}$ and asymmetry coefficient $\bar{\alpha}$. There is an overall tendency for $\bar{\epsilon}$ to decrease with the length L of the tubule (and, therefore, increase with the bending stiffness β, since in the rescaled variables β is proportional to L^{-4}).

As $\beta \to \infty$, $\bar{\epsilon}$ approaches the stiff limit value 0.63; see Eq. (4). In contrast, dwelling of the motors at the tubule ends has a relatively small effect on the inelasticity if the tubules are sufficiently stiff, although it may affect other properties of the interaction [9].

A decrease of the stiffness induces a significant asymmetry of the inelasticity with respect to the location of the initial attachment point s_i, as measured by the asymmetry coefficient $\bar{\alpha}$. However, our calculations show that $\bar{\alpha}$ remains relatively small for typical filament lengths used in the majority of experiments ($\bar{\alpha} < 0.03$). This result suggests that the kernel anisotropy related to dwelling of the motors [9] is the dominant factor affecting the large-scale pattern selection.

The dependence of the mean inelasticity $\bar{\epsilon}$ and its asymmetry $\bar{\alpha}$ on the tubule length and, hence, the effective stiffness are illustrated in Figs. 8–9.

For very large rod lengths, $\bar{\epsilon}$ approaches the value 0.42. Surprisingly, the dependencies are not monotonic for the no-dwelling case. This observation is likely related to the buckling of the rods when the filament length exceeds a certain critical value.

B. Bending of Actin Filaments

The same approach can be applied to much softer filaments, such as actin. The stiffness of actin is about 1000 times smaller than that of microtubules ($\beta = 7.3 \times 10^{-2}$ pN μm^2). Preliminary simulations indicate that the interaction of the motor with two actin filaments results in the creation of complex multilooped structures shown in Fig. 10. These loops are the result of an Euler bending instability of the elastic rods. As loops form, the tension g becomes negative and exhibits oscillating behavior; see Fig. 11. After the motor reaches the end of the filaments, buckling slowly relaxes because of the filament flexibility. Moreover, dwelling can have a significant effect on the inelasticity factor because of very slow straightening of the filaments; see Fig. 10. Complex structures shown in Fig. 10 may appear in the course of cytoskeleton formation and should affect the rheological properties of the filament networks. Note that actin filaments take significantly longer to relax back to the unbent configuration because of their much smaller stiffness. Thus, the notion of inelastic collision, which was introduced for stiff microtubules, is essentially inapplicable to actin. The formation of loops in actin filaments should facilitate multiple motor bindings and thus the creation of bundles. Dynamics of actin filaments will be examined in more detail in a forthcoming publication.

IV. CONCLUSIONS

In this paper we have investigated the interaction of a pair of biofilaments (microtubules, actin) mediated by a molecular motor. Our main result is that bending effects significantly amplify the tendency of microtubules to align and, consequently, to form structures with large-scale ordering, such as asters and vortices. Our results support the observations made in Refs. [4, 5] that bending effects are important for the explanation of self-organization processes in molecular motor–microtubule mixtures. Our preliminary studies indicate that molecular motors have a very strong effect on the shape of much softer filaments like actin, resulting in surprising Euler buckling instabilities and the formation of multi-loop structures. Presumably, these effects have a strong influence on the rheological properties of interconnected actin networks interacting with myosin motors.

We thank Jacques Prost, Francois Nédélec, Frank Jülicher, and Karsten Kruse for useful discussions. This work was supported by the U.S. Department of Energy, grants DE-AC02-06CH11357 (DK,HGK,IA) and DE-FG02-04ER46135 (LT).

APPENDIX A: SYMMETRIC ATTACHMENT LIMIT

In this appendix we show that the tendency for a pair of stiff filaments (microtubules) to orient themselves perpendicular to their bisector persists even in the case of non-zero length motors. The filaments are assumed to be of the same length, with the motor attached at an equal distance from the minus end of each filament (*even* attachment) and oriented transversally to the bisector of the filament pair (*symmetric* attachment). The general idea of symmetrization of motor attachment is captured in the case of rigid tubules connected by a stiff (but flexible) motor of length h where $h \ll L$. The motion then reduces to a system of ordinary differential equations governing the overdamped motion of a system of two rigid rods (microtubules) connected by flexible inextensible link of the length h (motor) as depicted in Fig. 12.

In a fixed coordinate system the centers of mass of the tubules are at $\mathbf{c}^{(1)}$ and $\mathbf{c}^{(2)}$, respectively, while the motor attachment points are at $\mathbf{c}^{(1)} + \mathbf{t}^{(1)}$ and $\mathbf{c}^{(2)} + \mathbf{t}^{(2)}$. In terms of the distances from the respective centers $s_{1,2}$ we have $\mathbf{t}^{(1,2)} = s_{1,2}\,\hat{\mathbf{t}}^{(1,2)}$. The motor is represented by the vector $\boldsymbol{\tau}$; $\mathbf{n}^{(1)}$, $\mathbf{n}^{(2)}$, and $\boldsymbol{\nu}$ are normal to $\mathbf{t}^{(1)}$, $\mathbf{t}^{(2)}$, and $\boldsymbol{\tau}$ respectively; and hats denote unit vectors.

The dynamics of the system are determined as in the semiflexible case by the balance of forces and the kinematic constraint $\frac{d}{dt}s_{1,2} = v$,

$$\frac{d}{dt}\mathbf{c}^{(1,2)} = \pm f\Big(\xi_{||}^{-1}(\hat{\mathbf{t}}^{(1,2)}, \hat{\boldsymbol{\tau}})\,\hat{\mathbf{t}}^{(1,2)} + \xi_{\perp}^{-1}(\hat{\mathbf{n}}^{(1,2)}, \hat{\boldsymbol{\tau}})\hat{\mathbf{n}}^{(1,2)}\Big),$$
$$\frac{d}{dt}\mathbf{t}^{(1,2)} = v\,\hat{\mathbf{t}}^{(1,2)} \pm f\xi_r^{-1}{s_{1,2}}^2[\hat{\mathbf{t}}^{(1,2)}, \hat{\boldsymbol{\tau}}]\,\hat{\mathbf{n}}^{(1,2)}, \qquad \text{(A1)}$$

where $\xi_{||}^{-1}$, $\xi_{\perp}^{-1}$, and ξ_r^{-1} denote the inverses of tangential, transversal, and rotational viscosities; the motor force of

magnitude f is directed along $\hat{\boldsymbol{\tau}}$, the sign depending on the direction from the tubule.

To obtain the force f and the motor motion, observe the geometric constraint $\boldsymbol{\tau} = (\mathbf{c}^{(2)} - \mathbf{c}^{(1)}) + (\mathbf{t}^{(2)} - \mathbf{t}^{(1)})$ (Fig. 12). Since the motor is rigid, its velocity must be directed along the normal $\hat{\boldsymbol{\nu}}$. Since the motor is rigid, its velocity is directed along the normal: $\dot{\boldsymbol{\tau}} = h\dot{\theta}\hat{\boldsymbol{\nu}}$. Here $\dot{\theta}$ denotes the angular velocity, which is independent of the choice of an orthonormal coordinate system. We obtain the relations

$$\begin{aligned} h\dot{\theta}\hat{\boldsymbol{\nu}} &= -f\xi_{||}^{-1}\Big((\hat{\mathbf{t}}^{(1)}, \hat{\boldsymbol{\tau}})\,\hat{\mathbf{t}}^{(1)} + (\hat{\mathbf{t}}^{(2)}, \hat{\boldsymbol{\tau}})\,\hat{\mathbf{t}}^{(2)}\Big) \\ &- f\xi_{\perp}^{-1}\Big((\hat{\mathbf{n}}^{(1)}, \hat{\boldsymbol{\tau}})\,\hat{\mathbf{n}}^{(1)} + (\hat{\mathbf{n}}^{(2)}, \hat{\boldsymbol{\tau}})\,\hat{\mathbf{n}}^{(2)}\Big) + v(\hat{\mathbf{t}}^{(2)} - \hat{\mathbf{t}}^{(1)}) \\ &- f\xi_{r}^{-1}\Big(s_1^2[\hat{\mathbf{t}}^{(1)}, \hat{\boldsymbol{\tau}}]\,\hat{\mathbf{n}}^{(1)} + s_2^2[\hat{\mathbf{t}}^{(2)}, \hat{\boldsymbol{\tau}}]\,\hat{\mathbf{n}}^{(2)}\Big). \end{aligned} \tag{A2}$$

Denote by $\mathbf{v}_{\hat{\mathbf{u}}} = (\mathbf{v},\ \hat{\mathbf{u}})\,\hat{\mathbf{u}}$ the component of a vector $\mathbf{v}$ along the unit vector $\hat{\mathbf{u}}$. Projecting the constraint (A2) onto the motor furnishes an equation for f independent of the motor size [18],

$$\begin{aligned} 0 = f\Big(&\xi_{||}^{-1}\big(|\hat{\boldsymbol{\tau}}_{\hat{\mathbf{t}}^{(1)}}|^2 + |\hat{\boldsymbol{\tau}}_{\hat{\mathbf{t}}^{(2)}}|^2\big) + \xi_{\perp}^{-1}\big(|\hat{\boldsymbol{\tau}}_{\hat{\mathbf{n}}^{(1)}}|^2 + |\hat{\boldsymbol{\tau}}_{\hat{\mathbf{n}}^{(2)}}|^2\big) \\ &+\xi_{r}^{-1}\big(s_1^2|\hat{\boldsymbol{\tau}}_{\hat{\mathbf{n}}^{(1)}}|^2 + s_2^2|\hat{\boldsymbol{\tau}}_{\hat{\mathbf{n}}^{(2)}}|^2\big)\Big) + v\big(\hat{\mathbf{t}}^{(2)} - \hat{\mathbf{t}}^{(1)}, \hat{\boldsymbol{\tau}}\big). \end{aligned}$$

The coefficient of f vanishes only if $\boldsymbol{\tau}$ is normal to both tangential and both normal vectors of the tubules, a condition that is clearly impossible even in the case of alignment. Hence, the force f is uniquely determined from the above relation and is $\mathcal{O}(1)$ relative to the motor size.

To determine the relative position of the motor and the tubules, we project the constraint (A2) onto $\hat{\mathbf{t}}^{(1)} + \hat{\mathbf{t}}^{(2)}$, which is along the tubule bisector. This eliminates the term with v (a rhombus has orthogonal diagonals),

$$f^{-1}h\dot{\theta}\Big(\hat{\boldsymbol{\nu}}, \hat{\mathbf{t}}^{(2)} + \hat{\mathbf{t}}^{(1)}\Big) = \xi_{||}^{-1}\Big(1 + \big(\hat{\mathbf{t}}^{(1)}, \hat{\mathbf{t}}^{(2)}\big)\Big)\Big(\hat{\mathbf{t}}^{(1)} + \hat{\mathbf{t}}^{(2)},\, \hat{\boldsymbol{\tau}}\Big) + \xi_{\perp}^{-1}\Big(\hat{\mathbf{t}}^{(2)}_{\hat{\mathbf{n}}^{(1)}} + \hat{\mathbf{t}}^{(1)}_{\hat{\mathbf{n}}^{(2)}},\, \hat{\boldsymbol{\tau}}\Big) + \xi_{r}^{-1}\Big(s_1^2\hat{\mathbf{t}}^{(2)}_{\hat{\mathbf{n}}^{(1)}} + s_2^2\hat{\mathbf{t}}^{(1)}_{\hat{\mathbf{n}}^{(2)}},\, \hat{\boldsymbol{\tau}}\Big) \tag{A3}$$

For finite h this relation determines the rotation rate of the motor $\dot{\theta}$ in terms of f. However, in the limit $h \to 0$ the motor becomes slaved to the tubules, with its orientation determined from the above relation with a zero left-hand side and irrespective of the force.

As discussed above, in this paper we consider the case of even attachment of the motor, where $s_1 = s_2 = s = (s_1+s_2)/2$. Simple algebra [19] shows that $\hat{\mathbf{t}}^{(2)}_{\hat{\mathbf{n}}^{(1)}} + \hat{\mathbf{t}}^{(1)}_{\hat{\mathbf{n}}^{(2)}} = \big(1 - (\hat{\mathbf{t}}^{(1)},\, \hat{\mathbf{t}}^{(2)})\big)\,(\hat{\mathbf{t}}^{(1)} + \hat{\mathbf{t}}^{(2)})$, and in the limit $h \to 0$ we obtain the condition

$$\Big(\hat{\mathbf{t}}^{(1)} + \hat{\mathbf{t}}^{(2)},\, \hat{\boldsymbol{\tau}}\Big) = 0 \tag{A4}$$

which means that $\hat{\boldsymbol{\tau}}$ is orthogonal to the bisector of the tubules—that is, the attachment becomes symmetric. Moreover, for $h \neq 0$, even if the motor initially was not perpendicular the bisector, Eq. (A3) describes the relaxation of the motor orientation toward the angle given by condition (A4).

APPENDIX B: DISCRETIZATION

We apply the finite element method (FEM) [20] to the weak form of the governing equations (8). This allows us to treat the singular terms arising from the motor force and automatically generates appropriate natural boundary conditions.

At any time t the components of the radius vector $\mathbf{r}(t)$ and its variation $\delta\mathbf{r}(t)$ are written as linear combinations of continuously differentiable functions $\phi_{j,k}$, $j = 0, \ldots, N-1$, $k = 0, 1$. The basis functions $\phi_{j,k}$ vanish outside the segments $[s_{j-1},\, s_{j+1}]$, $j = 0, \ldots, N$ centered at the nodes of a one-dimensional mesh discretizing the normalized tubule $[-1/2,\, 1/2]$ with the mesh size $\Delta s = s_{j+1} - s_j = 1/N$. We construct the basis from the standard Hermite cubics: $\phi_{j,k}$ are piecewise cubic polynomials on each mesh interval and $\phi_{j,0}$ interpolate function values while $\phi_{j,1}$ interpolate derivative values. On the interval $[-1,\, 1]$ the standard Hermite functions $\hat{\phi}_k, k = 0, 1$ have the form (see [20])

$$\hat{\phi}_0(s) = (|s| - 1)^2(2|s| + 1), \quad \hat{\phi}_1(s) = s(|s| - 1)^2,$$

from which the basis functions are obtained by shifting and scaling:

$$\phi_{j,k}(s) = \hat{\phi}_k\left((s - s_j)/\Delta s\right).$$

Similarly, the tension $g(t)$ and its variation $\delta g(t)$ are expanded by using the basis of piecewise linear "hat" functions ξ_j centered at the mesh nodes obtained from the standard hat function on $[-1,\, 1]$:

$$\hat{\xi}(s) = 1 - |s|, \quad \xi_j(s) = \hat{\xi}\left((s - s_j)/\Delta s\right).$$

For the end nodes $j = 0, N$ both ξ_j and $\phi_{j,k}$ are the suitable one-sided restrictions.

The Galerkin procedure requires that the approximate solution

$$\hat{\mathbf{r}}(s,t) = \sum_{j,k} \hat{\mathbf{r}}_{j,k}(t)\phi_{j,k}(s),\ \hat{g}(s,t) = \sum_{j} \hat{g}_j(t)\xi_j(s)$$

and $\hat{\mathbf{f}}(t)$ satisfy Eqs. (9)–(10) for all piecewise cubics $\delta\hat{\mathbf{r}}$, all piecewise linear functions $\delta\hat{g}$, and all scalars $\delta\hat{\mathbf{f}}$. As discussed in Section II B, this choice of the discretization space contains a suitable weak form of the boundary conditions (11). The resulting discrete equations can be viewed as the application of D'Alembert's principle to the energy functional (7) restricted to this finite-dimensional function space of piecewise cubic tubule conformations and piecewise linear tension profiles. The gradient flow and constraints thus generated are well-posed ordinary differential equations with discrete inextensibility and motor attachment constraints.

To write down these equations explicitly, we introduce the familiar mass and bending matrices $\mathbf{M}$ and $\mathbf{B}$, as well as a nonlinear version of the stiffness matrix $\mathbf{K}(\hat{g})$:

$$\begin{aligned} M_{j,k;j',k'} &= \int_{-L/2}^{L/2} \phi_{j,k}\phi_{j',k'}\,ds, \\ B_{j,k;j',k'} &= \int_{-L/2}^{L/2} \left(\partial_s^2\phi_{j,k}\right)\left(\partial_s^2\phi_{j',k'}\right) ds, \\ K_{j,k;j',k'}(\hat{g}) &= \sum_i \hat{g}_i K_{i;j,k;j',k'} = \int_{-L/2}^{L/2} \phi_{j,k}\phi_{j',k'}\hat{g}_i\xi_i\,ds. \end{aligned}$$

With these, the implicit Euler's scheme at a succession of times t_n produces a system of discrete equations,

$$\begin{aligned} &\sum_{j',\,k'} 2\Big(\eta M_{j,k;j',k'}(\hat{\mathbf{r}}^{n+1}_{j',k'} - \hat{\mathbf{r}}^{n}_{j',k'})(t_{n+1}-t_n) \\ &\quad + K_{j,k;j',k'}(\hat{g})\hat{\mathbf{r}}^{n+1}_{j',k'} + B_{j,k;j',k'}\hat{\mathbf{r}}^{n+1}_{j',k'}\Big) \\ &\quad + \hat{\mathbf{f}}^{n+1}\phi_{j,k}(s_a(t^{n+1})) = 0, \qquad \text{(B1)} \\ &\sum_{j,\,k;j',\,k'} K_{i;j,k;j',k'}\hat{\mathbf{r}}_{j,k}\hat{\mathbf{r}}_{j',k'} = 0, \qquad \text{(B2)} \\ &\sum_{j',\,k'} \hat{\mathbf{r}}_{j',k'}\phi_{j',\,k'}(s_a(t)) = 0, \qquad \text{(B3)} \end{aligned}$$

which are solved numerically for all i, j, k,

For our numerical studies we start with the initial state of a relaxed tubule forming a given angle $\frac{1}{2}\varphi^0$ with the vertical axis. For a given motor attachment point $s_a^0 \in [-\frac{1}{2}, \frac{1}{2}]$ the following discrete conformation determines a normalized symmetric tubule pair with the initial angle φ^0 and the intersection point at the origin:

$$\begin{aligned} \hat{\mathbf{r}}_{j,0} &= \Big(\cos(\varphi^0/2),\, \sin(\varphi^0/2)\Big)(j\Delta s - s_a^0), \\ \hat{\mathbf{r}}_{j,1} &= \Big(\cos(\varphi^0/2),\, \sin(\varphi^0/2)\Big). \end{aligned}$$

Initially the tension and the motor force are absent, $\hat{g}_i^0 = 0$, $\mathbf{f}^0 = \mathbf{0}$.

The conformation $\hat{\mathbf{r}}^n_{j,k}$ along with the tension $\hat{g}_i^n$ and the force $\mathbf{f}^n$ at a later time t_n are determined by solving the nonlinear equations (B1)–(B3) recursively. At each time t_{n+1} these equations are solved by using Newton's method with the state at time t_n serving as the initial guess. The corresponding linearized system is sparse and can be efficiently solved using any Krylov subspace method. For modest N the standard LU-factorization is also feasible.

[1] J. Howard, *Mechanics of Motor Proteins and the Cytoskeleton*, Springer, New York, 2000.
[2] K.Takiguchi, J.Biochem. (Tokyo) **109**, 250 (1991)
[3] R. Urrutia, M.A. McNiven, J.P. Albanesi, D.B. Murphy, B. Kachar, Proc. Natl. Acad. Sci. USA **88**, 6701 (1991).
[4] F.J. Nédélec, T. Surrey, A. C. Maggs, and S. Leibler, Nature (London) **389**, 305 (1997).
[5] T. Surrey, F. Nédélec, S. Leibler, and E. Karsenti, Science, **292**, 1167 (2001).
[6] D. Humphrey, C. Duggan, D. Saha, D. Smith, and J. Käs, Nature (London) **416**, 413 (2002).
[7] F. Nédélec, T. Surrey, A.C. Maggs, Phys. Rev. Lett. **86**, 3192 (2001)
[8] I.S. Aranson, L.S. Tsimring, Phys. Rev. E **71**, 050901(R) (2005)
[9] I.S. Aranson, L.S. Tsimring, Phys. Rev. E **74**, 031915 (2006)
[10] E. Ben-Naim and P. L. Krapivsky, Phys. Rev. E **73**, 031109 (2006)
[11] I. Goldhirsh and G. Zanetti, Phys. Rev. Lett. **70**, 1619 (1993)
[12] I.S. Aranson, L.S. Tsimring, Rev. Mod. Phys. **78**, 641 (2006)
[13] P. Ranjith, P. Kumar, Phys. Rev. Lett. **89**, 018302 (2002)
[14] T. Munk, O. Hallatschek, Ch. H. Wiggins, and E. Frey, Phys. Rev. E **74** , 041911 (2006)
[15] F. Gittes, B. Mickey, J. Nettleton, J. Howard, J. Cell Bio., **120**, 923 (1993)
[16] C. Brennen, H. Winet, Ann. Rev. Fluid Mech, **9**, 339 (1977)

[17] L.D. Landau and E.M. Lifshits, *Theory of Elasticity*, London, Pergamon Press; Reading, Mass., Addison-Wesley Pub. Co., 1959

[18] In two dimensions a vector product of a vector with $\hat{\boldsymbol{\tau}}$ is a scalar, and can be replaced by a scalar product of the normal with $\hat{\boldsymbol{\tau}}$ (see illustration on the right of Fig. 12).

[19] We have $\hat{\mathbf{t}}^{(1)} + \hat{\mathbf{t}}^{(2)} = \hat{\mathbf{t}}^{(1)}_{\hat{\mathbf{t}}^{(2)}} + \hat{\mathbf{t}}^{(1)}_{\hat{\mathbf{n}}^{(2)}} + \hat{\mathbf{t}}^{(2)}_{\hat{\mathbf{t}}^{(1)}} + \hat{\mathbf{t}}^{(2)}_{\hat{\mathbf{n}}^{(1)}} = \hat{\mathbf{t}}^{(1)}_{\hat{\mathbf{n}}^{(2)}} + \hat{\mathbf{t}}^{(2)}_{\hat{\mathbf{n}}^{(1)}} + (\mathbf{t}^{(1)}, \mathbf{t}^{(2)})(\hat{\mathbf{t}}^{(1)} + \hat{\mathbf{t}}^{(2)})$.

[20] G. Strang, G. Fix, *An Analysis of the Finite Element Method*, Prentice-Hall, 1973

[21] See EPAPS Document No. # or website *http://www-unix.mcs.anl.gov/dynamics/multiscale/sf* for computer animations of simulations results. A direct link to this document can be found in the reference section of the online HTML version of the present article. The document can also be reached via the EPAPS homepage (http://www.aip.org/pubservs/epaps.html) or from ftp.aip.org in the directory /epaps/. See the EPAPS homepage for more information.

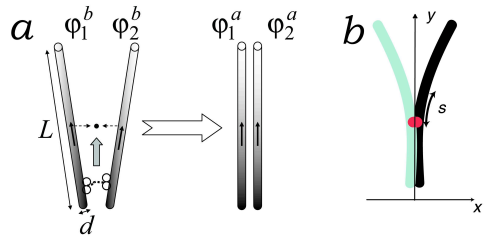

FIG. 1: (Color online) (a) A fully inelastic collision of two microtubules mediated by a molecular motor. (b) Schematic representation: The molecular motor is attached symmetrically to two flexible microtubules at a distance s along the tubule from the midpoint.

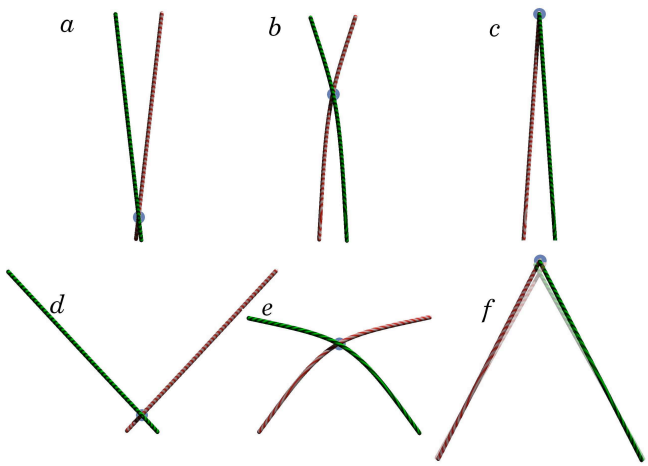

FIG. 2: (Color online) Two sequences of images illustrating the bending and alignment of microtubules by molecular motors, with dwelling of the motor at the end of the microtubules. (a–c) Initial angle $\varphi_0 = 14^\circ$, (d–f) Initial angle $\varphi_0 = 90^\circ$. The shaded region indicates the motor location; the motor moves upward. For comparison purposes, the image (f) also shows the configuration of the two microtubules if the dwelling time is zero (shown by semitransparent colors). The sequence shows the configurations at times $t = 3$ (a,d), $t = 33$ (b,e), and $t = 180$ (c,f) for $\beta = 20$ pN μm^2, $L = 60$ μm, motor velocity $v = 1\mu$m/s, and initial attachment offset 6μm from the tubule end. After the interaction with the motor, the initial angle is reduced from 14° to 8.7° with dwelling and from 90° to 58.3° with dwelling and to 62.2° without dwelling (shaded). More detailed images can be found in [21, Movies 1 and 2].

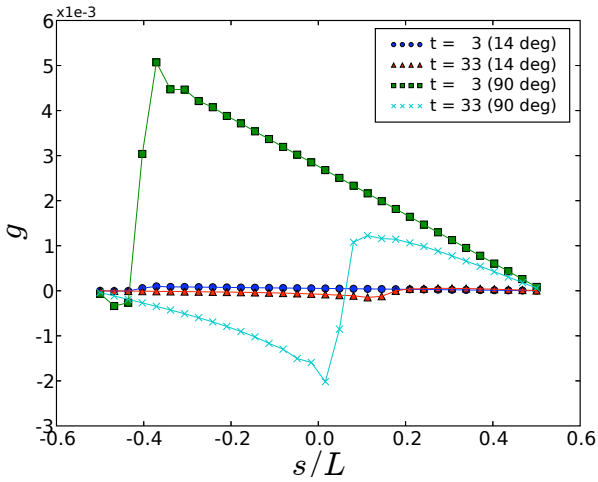

FIG. 3: (Color online) Tension in the tubule configurations of Fig. 2 at times $t = 3$ (a,d) and $t = 33$ (b,e); $\beta = 20$ pN μm^2, $L = 60\mu$m, $v = 1\mu$m/s. At the final stages (e,f), the tension is zero (not shown). The tension g changes sign and varies very rapidly near the motor attachment point. A smaller initial angle ($\varphi_0 = 14^\circ$) results in a tension that is approximately 10 times smaller than the larger initial angle (90°).

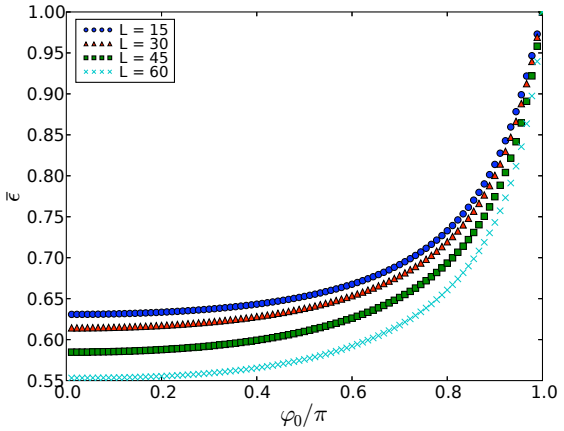

FIG. 4: (Color online) Inelasticity factor $\bar{\epsilon}$ with dwelling, for different lengths of microtubules; $\beta = 20$ pN μm^2.

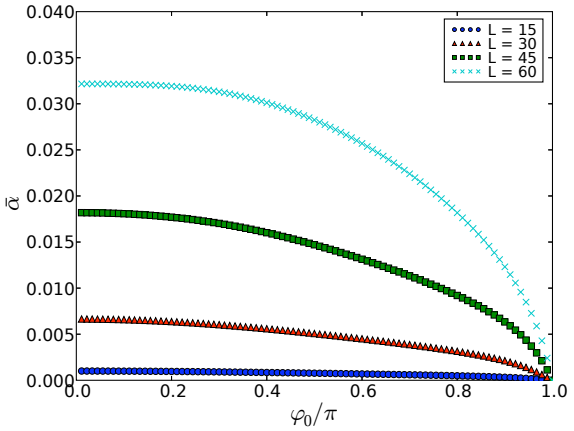

FIG. 5: (Color online) Asymmetry coefficient $\bar{\alpha}$ with dwelling, for different lengths of microtubules; $\beta = 20$ pN μm^2.

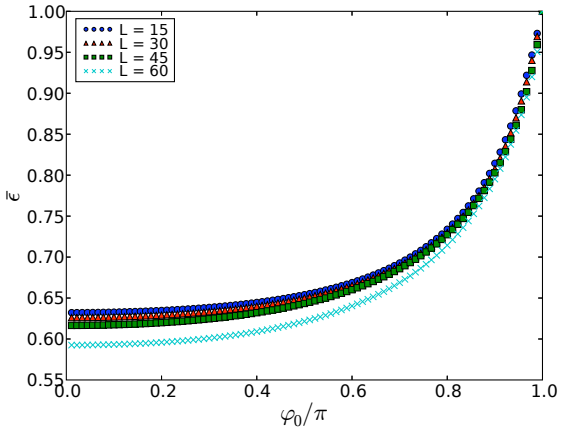

FIG. 6: (Color online) Inelasticity factor $\bar{\epsilon}$ without dwelling as a function of the tubule length; $\beta = 20$ pN μm^2.

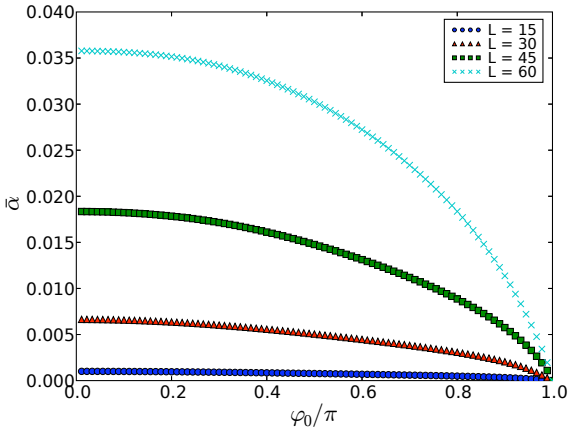

FIG. 7: (Color online) Asymmetry coefficient $\bar{\alpha}$ without dwelling as a function of the tubule length; $\beta = 20$ pN μm^2.

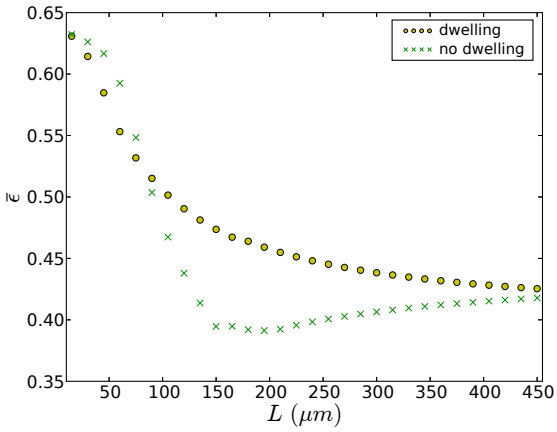

FIG. 8: (Color online) Inelasticity factor for $\varphi_0 = 4°$ as a function of the tubule length (and, by implication, as a function of the effective bending stiffness of a unit tubule); $\beta = 20$ pN μm^2.

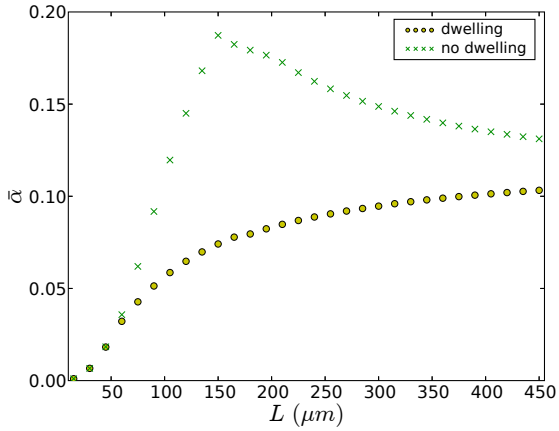

FIG. 9: (Color online) Asymmetry coefficient $\bar{\alpha}$ for $\varphi_0 = 4^\circ$ as a function of tubule length (and, by implication, as a function of the effective bending stiffness of a unit tubule); $\beta = 20$ pN μm^2.

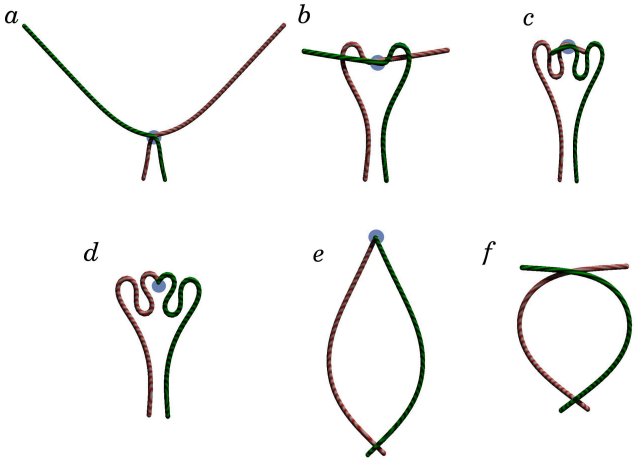

FIG. 10: (Color online) Two sequences of images illustrating the bending and alignment of actinlike filaments by molecular motors: (a–d) with motor in motion, (e) with motor dwelling at the end of the filaments after interaction, and (f) filaments freely relaxing after interaction. The shaded region indicates the motor location; the motor moves upward. Images are shown at times $t = 1.5$ (a), $t = 9$ (b), $t = 12.5$ (c) $t = 13.5$ (d), and $t = 100.0$ (e,f); $\beta = 7.3 \times 10^{-2}$ pN μm^2, $L = 15\mu$m, and $v = 1\mu$m/s. The images (e,f) illustrate the difference between dwelling and nondwelling interactions. In both cases, the initial angle is $\varphi_0 = 90^\circ$ and the initial attachment offset is $1\mu m$ from the end of the filament. After the interaction with the motor, the initial angle is reduced to 19.9° with dwelling and to 32.7° without dwelling. More detailed images can be found in [21, Movies 3 and 4].

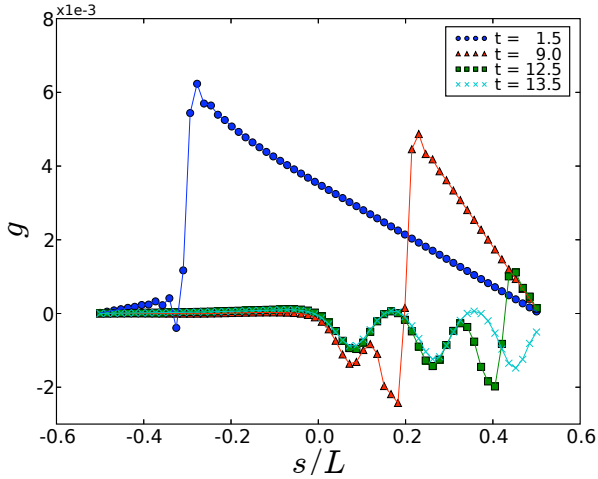

FIG. 11: (Color online) Tension in the tubule configurations of Fig. 10 at times $t = 1.5$ (a), $t = 9$ (b), $t = 12.5$ (c) $t = 13.5$ (d); $\beta = 7.3 \times 10^{-2}$ pN μm^2, $L = 15\mu$m, $v = 1\mu$m/s. With the motor attached near the very end ($t = 13.5$), the tension has an oscillatory profile which decays rapidly to an essentially tension-free profile ($g \approx 0$, not shown), regardless of whether the motor is still attached (dwelling) or not (without dwelling).

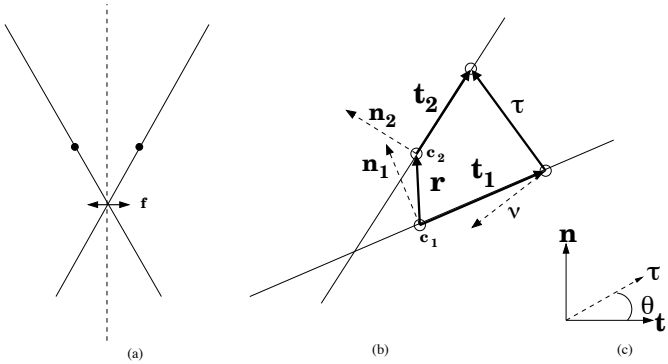

FIG. 12: Initial state of a symmetric microtubule pair: force acts on the microtubules perpendicular to bisector, attachment point equidistant from centers of mass (a); inflexible tubules connected by a finite-size motor (b); a vector in an orthonormal frame (c).